Hydrogen adsorption and hydrogen evolution reaction on a polycrystalline Pt electrode studied by surface-enhanced infrared absorption spectroscopy

Keiji Kunimatsu,[a,†] Takahiro Senzaki,[b] Gabor Samjeské,[a,c] Minoru Tsushima,[a,c] Masatoshi Osawa[a,*]

[a] Catalysis Research Center, Hokkaido University, Sapporo 001-0021, Japan

[b] Graduate School of Environmental Earth Science, Hokkaido University, Sapporo 060-0810, Japan

[c] CREST, Japan Science and Technology Agency, Kawaguchi, Saitama 332-0012, Japan

* Corresponding author. Phone: +81-11-706-9123; Fax: +81-11-706-9124; E-mail: osawam@cat.hokudai.ac.jp (M. Osawa)

† Present address: Clean Energy Research Center, University of Yamanashi, 7-32 Miyamae-cho, Kofu, 400-0021 Japan

Abstract

Hydrogen evolution reaction (HER) on a polycrystalline Pt electrode has been investigated in Ar-purged acids by surface-enhanced infrared absorption spectroscopy and electrochemical kinetic analysis (Tafel plot). A vibrational mode characteristic to H atom adsorbed at atop sites (terminal H) was observed at 2080–2095 cm^{-1}. This band appears at 0.1 V (RHE) and grows at more negative potentials in parallel to the increase in hydrogen evolution current. Good signal-to-noise ratio of the spectra enabled us to establish the quantitative relation between the band intensity (equivalently, coverage) of terminal H and the kinetics of HER, from which we conclude that terminal H atom is the reaction intermediate in HER and the recombination of two terminal H atoms is the rate determining step. The quantitative analysis of the infrared data also revealed that the adsorption of terminal H follows the Frumkin isotherm with repulsive interaction.

Keywords: Electrocatalysis; Hydrogen adsorption; Hydrogen evolution reaction; Pt; IR spectroscopy

1. Introduction

Hydrogen adsorption and hydrogen evolution reaction (HER) on metal electrodes are the most fundamental issues in electrochemistry and have been studied extensively [1-8]. This subject is important also in surface science and heterogeneous catalysis [9].

It is generally accepted that HER occurs via two successive steps; the initial discharge of hydronium ion (H_3O^+) to give adsorbed hydrogen atom H(a) (Volmer step)

$$H_3O^+ + e^- \leftrightarrow H(a) + H_2O \quad (1)$$

followed by recombination of two adsorbed H atoms (Tafel step)

$$2H(a) \rightarrow H_2 \quad (2)$$

or a reaction of adsorbed H with H_3O^+ in the solution (Heyrovsky step)

$$H(a) + H_3O^+ + e^- \rightarrow H_2 + H_2O \quad (3)$$

yielding H_2. The kinetics of HER exhibits a Tafel slope of ca 30mV/decade commonly on Pt(poly), (111), (110) and (100) in acidic media [3,7,10-13], from which HER on Pt in acidic media is generally believed to occur via the Volmer-Tafel mechanism with the latter being rate-determining [1-3]. However, recent studies using rotating single-crystal electrodes suggested that the kinetics depends on crystallographic orientation of the electrode surface [6,14,15]. The Volmer-Tafel and Volmer-Heyrovsky mechanisms were proposed for Pt(110) and Pt(100), respectively [6,14].

Hydrogen adsorption on Pt at potentials positive of the thermodynamic reversible potential of HER (E_{eq}), i.e. underpotential deposition (upd), has been well established [4,5,8]. The HER occurs at less positive potentials where the electrode surface has been fully covered by upd hydrogen (H_{upd}). This fact was interpreted that the intermediate in HER is not H_{upd} but overpotentially deposited hydrogen, H_{opd} [3,4]. However, it should be noted that H_{opd} is a thermodynamic notation introduced by Conway [4,5] and does not specify any adsorbed state of H. The nature of the reaction intermediate and its relation to the reaction mechanism have

not been fully understood yet.

Vibrational spectroscopy is one of the most useful techniques to characterize reaction intermediates in surface reactions. Nichols and Bewick [16,17] applied infrared reflection-absorption spectroscopy (IRAS) to the study of H adsorption on Pt electrodes. The authors observed for the first time a very weak vibration at 2090 cm^{-1} on both polycrystalline and single-crystal Pt surfaces and assigned this band to the Pt–H vibration, ν(Pt–H), of H atoms adsorbed at atop sites on Pt (terminal H). This band appears around 0.1 V (RHE) and increases in intensity as the potential is made less positive in parallel to the increase in the current of HER. From the potential dependence of the band intensity, they suggested that terminal H is the reaction intermediate in HER. Similar vibrations were observed also on Rh and Ir surfaces at almost the same frequency [16,17].

The IRAS result was interpreted as a strong support to the structure insensitive kinetics of HER [7,9-13]. However, the IRAS work was not fully reproduced in the succeeding *in situ* IRAS and visible-infrared sum-frequency generation (SFG) studies on polycrystalline and single-crystal Pt electrodes [18-21]. Ogasawara and Ito [18] observed a band at 2082 cm^{-1} on Pt(110) and at 2009-2020 cm^{-1} on Pt(100) by IRAS. The vibrational frequency observed on Pt(110) is close to the corresponding experiment by Nichols and Bewick (2090 cm^{-1}) [16,17], but that observed on Pt(110) is much lower. In addition, they did not observed any bands corresponding to adsorbed H atom on well-defined Pt(111). By using SFG, Tadjeddine and Peremans [20,21] observed two or three vibrations in the spectral range of 1900–2050 cm^{-1} and a vibration at ~1770 cm^{-1} on both polycrystalline and single-crystal Pt electrodes. The frequencies of these vibrations are slightly sensitive to the crystallographic orientation of the surface. They assigned the vibration around 1770 cm^{-1} to a dihydride, $Pt–H_2$, and suggested that the dihydride is the reaction intermediate in HER. The crystallographic dependence of the Pt–H vibration appear to support the structural dependence of the HER kinetics on

single-crystal electrodes. However, Nanbu et al. [19] suggested that the bands at 1900-2050 cm^{-1} and ~1800 cm^{-1} arise from CO adsorbed at atop and bridge sites, respectively, that are produced by the reduction of trace CO_2 in the solution.

In a recent study using surface-enhanced IR absorption spectroscopy (SEIRAS) with an attenuated total reflection (ATR) mode [22], we demonstrated that the IRAS study by Nichols and Bewick on polycrystalline Pt electrodes [16,17] is fully reproducible. It should be noted that the ATR-SEIRAS study was not a simple reinvestigation and differed from earlier vibrational spectroscopic studies regarding to two issues. First, the potential range examined was wider than that employed in the IRAS and SFG studies. In IRAS and SFG, the electrode surface was pushed against an IR transparent window to reduce the IR absorption by the solution. The thin layer configuration of the cell limited the measurements to the potential range where HER is slow (E > 27 mV vs RHE in Ref. [16]) because evolved H_2 gas is trapped in the thin layer cavity and disturbs both spectral and electrochemical measurements. High resistance of the thin layer cell is another problem: large ohmic drop prevents the polarization to more negative potentials. In contrast, IR radiation is introduced from the backside of the electrode through an IR transparent prism in the ATR setup, and thus H_2 gas evolution does not disturbs spectral and electrochemical measurements. Higher sensitivity is an additional advantage of ATR-SEIRAS over IRAS [23,24]. These advantages allowed us a quantitative analysis of the IR data over a wider potential range down to –30 mV. By comparing the IR data with the kinetics of HER (Tafel plot), we suggested that terminal H is actually the reaction intermediate in HER. Very recently, we showed that terminal H is the reaction intermediate also in hydrogen oxidation reaction (HOR) by using the same technique [25]. In the present manuscript, we will report further experimental results and discuss the mechanism of HER under inert atmosphere in more detail on the basis of the SEIRAS data.

2. Experimental

Experimental details of ATR-SEIRAS were given elsewhere [23,24,26-29]. The Pt working electrode was a thin (ca. 50 nm) film formed on the total reflecting plane of a hemicylindrical Si ATR prism by a chemical deposition technique [28,29]. The electrode surface was very smooth by eye inspection and as shiny as well-polished bulk electrodes. Auger electron spectroscopy and scanning electron microscopy analyses revealed that the Si substrate was fully covered by the chemically deposited Pt film.

A potentiostat (EG&G PARC model 263A) was used for controlling potential. The spectroelectrochemical cell used was a three-electrode design equipped with a H_2-trapped reversible hydrogen electrode (RHE) and a Pt mesh counter electrode [27]. To minimize ohmic drop (iR_u), the tip of a Luggin capillary was located a few mm away from the working electrode. Electrode potential was measured with respect to the RHE and is reported in this manuscript after correcting ohmic drop which was calculated from the observed current and the solution resistance R_u determined by the current interruption method [30]. The hydrogen evolution current used for constructing Tafel plot was recorded while conducting the SEIRAS measurement at given potentials.

The electrolyte solutions were prepared from ultrapur grade H_2SO_4, $HClO_4$ and HCl (Kanto Kagaku), and Millipore water with the TOC level less than 5 ppb. In some measurements, D_2O (99.9 atom % D, Aldrich) was used as the solvent instead of H_2O without further purification. The solutions were purged by high-purity Ar before and during the measurements. After setting the Pt-coated Si prism to the cell and filled out with the electrolyte, the electrode surface was cleaned by cycling potential between 0.05 and 1.5 V until a stable cyclic voltammogram (CV) was obtained. Almost no changes were observed in the CV after the surface cleaning, indicating that the solution was very clean.

A Bio-Rad FTS-60A/896 FT-IR spectrometer equipped with a liquid-N_2-cooled MCT detector and a homemade single-reflection accessory (incident angle of 60°) was used in recording SEIRA spectra at a spectral resolution of 4 cm^{-1}. Typically 200–500 interferometer scans were coadded to each spectrum to enhance the signal-to-noise ratio (S/N). The measurements were conducted with unpolarized IR radiation except otherwise noted. All spectra are shown in the absorbance units defined as $-\log (I_0/I)$, where I_0 and I represent the single-beam spectra at reference and sample potentials, respectively. The reference spectrum I_0 was measured in the double layer potential region (typically at 0.6 V) and then the sample spectrum was collected at a sample potential. The measurements were repeated by changing the sample potential stepwise to cover the H_{upd} and HER regions (between –0.06 and +0.4 V). Despite careful cleaning of the electrode surface and the use of high-purity solutions, the IR spectra of the electrode surface were often contaminated by very weak bands at ~2000 and ~1800 cm^{-1} assignable to linear- and bridge-bonded CO, respectively, that may be derived from organic impurities in the electrolyte solution (mostly trace CO_2 in the solution [19]). To obtain CO-free spectra, the platinum electrode was subjected to pre-polarization at 1.0 V for typically 10 s before recording each set of reference and sample spectra.

Although the spectrometer was purged by dry air or N_2, water vapor in the spectrometer gave rise to uncompensated bands in the most cases. These bands were subtracted from the observed spectra by using a spectrum of water vapor measured separately without the cell. The SEIRAS spectra below 900 cm^{-1} had poor S/N due to strong IR absorption by the Si prism and thus the results above 900 cm^{-1} are reported.

3. Results and discussion

3.1. Electrochemical measurements

A CV for a chemically deposited Pt film electrode measured in Ar-saturated 0.5 M H_2SO_4 at 50 mV s^{-1} is shown in Fig. 1. The voltammetric feature is very similar to that for bulk polycrystalline Pt electrodes [31]. The adsorption and desorption of H_{upd} exhibit characteristic peaks in the potential range between 0.1 and 0.4 V, and HER commences at about 50 mV. The true surface area of the electrode, determined from the charge for the desorption of H_{upd} by assuming 210 μC cm^{-2} for monolayer, was 11.87 cm^2, while the geometrical area of the electrode in contact with the solution was 1.77 cm^2. The large roughness factor of 6.7, calculated from the true and geometrical areas, stems from a granular structure of the Pt electrode surface in the nanometer-scale [29]. The nanometer-scale roughness plays a dominant role in enhancing the IR absorption of adsorbates [23,24,32]. Current densities shown hereafter were calculated with the true surface area.

The Tafel plots observed in 0.5 M H_2SO_4 and 1 M $HClO_4$ are presented in Fig. 2. The measurement in 0.5 M H_2SO_4 was limited down to –30 mV due to large current at less positive potentials. On the other hand, the higher conductivity (i.e. smaller R_u) of 1 M $HClO_4$ solution allowed the polarization down to –60 mV. The Tafel slop is close to 30 mV/decade in consistent with the literature data [3,7,10-13].

3.2. SEIRA spectra

3.2.1. Overall spectral features in the 4000 – 900 cm^{-1} range

Fig. 3 shows SEIRA spectra observed in 0.5 M H_2SO_4 at E = 0.12, 0.07, 0.03, and –0.03 V (from bottom to top) with respect to the reference potential of 0.6 V. The upward and downward peaks represent the increase and decrease, respectively, in intensity with respect to the reference potential. The downward bands between 1219 and 949 cm^{-1} are assigned to sulfate or bisulfate ions that were adsorbed at the reference potential and desorbed at the sample potentials [33,34]. The bipolar bands at 3700-2500 and 1620 cm^{-1} are assigned to the OH stretching, ν(OH), and HOH bending, δ(HOH), modes, respectively, of water molecules at the

interface [27, 35]. Since the spectrum of interfacial water depends on applied potential through the changes in orientation and interactions with coadsorbed ions [27,35], the water bands are bipolar in shape.

Besides, three upward bands that increase in intensity with decrease in potential are observed at 2090–2080, ~1700, and 1050 cm^{-1} (the last band is denoted by an arrow for clarity). The upward band at 2080–2090 cm^{-1} that appears around 0.1 V and grows in intensity at less positive potential has already been reported by Nichols and Bewick [16,17] and assigned to the ν(Pt–H) mode of terminal H. This band was observed also by Nanbu et al. [19] although their electrode surface was severely contaminated by CO. The potential dependent frequency shift clearly demonstrates that this band arises from adsorbed species. The band around 1700 cm^{-1} that grows as the potential is made more negative is the asymmetric δ(HOH) mode of H_3O^+ ion [27,35]. The H_3O^+ band appears to be shifted to lower frequencies as the potential is made more negative and merge into the δ(HOH) mode of water. The shift is suggestive of the adsorption of H_3O^+ on the electrode surface as the precursor for hydrogen absorption. The peak at 1050 cm^{-1} is discussed later.

The assignments of the two upward bands at 2080–2090 and ~1700 cm^{-1} to terminal H and H_3O^+, respectively, are supported by the isotopic shifts for the substitution of the solvent from H_2O to D_2O. Fig. 4 compares the spectra of the Pt electrode recorded in H_2O (a) and D_2O (b) solutions of 0.5 M H_2SO_4 at 0 V (versus RHE in the former and versus the reversible deuterium electrode, RDE, in the latter). The reference potential was 0.6 V for the former and 0.2 V for the latter. The lower reference potential for the latter was chosen to minimize the interference from the ν(OD) band of D_2O in the spectral range around 2100 cm^{-1} where ν(Pt–H) band is located. The 2085 cm^{-1} band in H_2O disappears in D_2O and a new band appears at 1498 cm^{-1}. The frequency ratio of the two bands, 2085/1498 = 1.39, is close to that theoretically predicted for ν(Pt-H) and ν (Pt-D) ($=\sqrt{m_D/m_H}$, where m_H and m_D are the

masses of H and D atoms, respectively). The slight deviation from √2 arises from the anharmonicity of the vibration [16]. The asymmetric δ(HOH) mode of H_3O^+ at ~1700 cm^{-1} also disappears in D_2O and a new band corresponding to the asymmetric δ(DOD) mode of D_3O^+ appears at about 1230 cm^{-1} (the shoulder of the δ(HOH) mode of D_2O at 1200 cm^{-1}). The upward peak at 1050 cm^{-1} also disappears by the solvent substitution.

3.2.2. Underpotentially deposited hydrogen, H_{upd}.

The CV (Fig. 1) shows that upd of H occurs at potentials less positive than 0.4 V, while terminal H is observed at potentials less positive than 0.12 V. Since E_{eq} of HER is more positive than 0 V in the Ar-saturated solution (E_{eq} = 0 V under the H_2 pressure of 1 atm), the terminal H corresponds to H_{upd} in the Conway's notation. On the other hand, H_{upd} is speculated to be located at hollow sites [8,14]. High-resolution energy loss spectroscopy (HR-EELS) and first-principle calculations showed that H atoms adsorbed at fcc three-fold hollow sites on Pt(111) exhibit dipole-allowed ν(Pt–H) modes at 113 and 153 meV (= 912 and 1234 cm^{-1}, respectively) in UHV [36]. The higher frequency mode has been observed also by IRAS in UHV (at 1254 cm^{-1}) [37]. Unfortunately, this spectral range is masked in H_2SO_4 by the bands of adsorbed (bi)sulfate. To examine this spectral range without the interference from adsorbed anions, we conducted the same experiment in 1 M HCl. The result obtained by using the reference potential of 0.4 V is shown in Fig. 5. The spectra in the 2250–1950 cm^{-1} range (left) shows that the adsorption of terminal H occurs at E < 0 V (0.1 V more negative than in H_2SO_4 and $HClO_4$ solutions due to the adsorption of Cl^- at E > 0 V [38]). In the lower frequency range of 1400–950 cm^{-1} (right), three features that change in intensity and/or frequency with applied potential are observed around 1250, 1100, and 980 cm^{-1}. The removal of the interference from the (bi)sulfate bands reveals that the true vibrational frequency of the 1050-cm^{-1} band observed in H_2SO_4 is 1100 cm^{-1}. The feature around 1250 cm^{-1} was observed also in $HClO_4$ (the 1000–1200 cm^{-1} range was masked by the ν(Cl–O) mode of perchlorate).

Among these three features, only the band at 1100 cm^{-1} were found to disappear when the solvent was changed from H_2O to D_2O, indicating that this band is ascribed to either adsorbed H or H_3O^+ [39] (H_2O has no absorption in this range). This band appears at about 0.2 V and monotonically grows as the potential is made more negative. The potential dependence of the intensity is different from that expected for H_{upd} and rather similar to that of the asymmetric δ(HOH) mode of H_3O^+ around 1700 cm^{-1} (Fig. 3). From this result, we tentatively assign the 1100-cm^{-1} band to the symmetric δ(HOH) mode of H_3O^+.

Since the feature around 1250 cm^{-1} is commonly observed also for other metals deposited on Si [35,40,41] and not on Ag and Cu deposited on Ge [42], this band may be assigned to a S-O stretching mode of Si oxide on the prism. The potential dependence of the bipolar feature may not be due to an electrochemical reaction because the prism was fully covered by the Pt thin film and not in direct contact with the solution. The feature at 980 cm^{-1} may be an artifact arising from the low transmittance of the Si prism.

In summary, we could not detect any signals definitely assignable to H_{upd}. This is probably due to its very small absorption coefficient [36,37] and/or the interference from the bands around 1250 and 1100 cm^{-1} of probably Si oxide and D_3O^+, respectively.

3.2.3. Influence of IR polarization state on the SEIRAS spectra

The peak intensity of the terminal H band around 2090 cm^{-1} is 4.4×10^{-4} absorbance at +30 mV (Fig. 3), while the corresponding value observed by IRAS at +27 mV is 1.2×10^{-4} in the differential reflectance change units $\Delta R/R$ (which corresponds to 5.2×10^{-5} absorbance) [16]. The 8.5-times larger band intensity observed by ATR-SEIRAS is partly ascribed to the difference in the roughness factors of the electrodes: it is 6.7 for the chemically deposited Pt film electrode and typically around 2 for mechanically polished surface. The estimated enhancement factor is no so significant, but it is noted that the SEIRA spectrum was collected with un-polarized radiation and the IRA spectrum was collected with p-polarized radiation.

For full comparison of the SEIRA and IRA spectra, the polarization dependence of the SEIRAS spectrum was examined. Fig. 6 shows the SEIRAS spectra of terminal H on Pt observed at 0.0 V in 3 M H_2SO_4 with s-, p- and un-polarized IR radiation. The peak intensity for p-polarization is 3.3 times as large as that for un-polarized radiation. Accordingly, the apparent enhancement factor of SEIRAS is calculated to be 28 (= 8.5 × 3.3) for p-polarization including the contribution of the larger surface area. The absence of any bands for s-polarization is due to the destructive interaction of the IR radiation within the metal film [26, 43].

3.3. Reaction intermediate in HER

The present ATR-SEIRAS study has clearly shown that the band assignable to terminal H appears at ~2090 cm^{-1} at a potential more negative than 0.12 V and increases its intensity as the potential is made more negative (Fig. 2). The increase in the band intensity is in parallel to the increase in HER current and strongly suggests that terminal H is the reaction intermediate in HER, as originally proposed by Nicohls and Bewick [16,17]. However, the potential dependence of the band intensity is not enough to conclude terminal H being the reaction intermediate. A further proof of this is obtained from the quantitative comparison of the SEIRAS data and the kinetics of HER, as is discussed in the following.

3.3.1. Terminal H

For the quantitative analysis of the SEIRAS data, the spectra in the 2250-1900 cm^{-1} range are reproduced in Fig. 7 by subtracting the tilted baselines. The band is very broad and almost symmetric. The broad band shape is intrinsic to the ν(Pt–H) vibration of terminal H and not due to the inhomogeneity of the polycrystalline surface because this band is as broad as on single crystal surfaces [17]. This is also the case for H atoms adsorbed at hollow sites on Pt(111) in UHV [36,37]. Since H atoms are known to be very mobile on metal surfaces [9], surface diffusion and/or the fluctuation of H atoms around adsorption sites may be the origin

of the broad feature of the ν(Pt–H) vibration.

In addition to the terminal H band, a very weak band is observed around 2000 cm^{-1} at 0.1 and 0.12 V (indicated by an arrow in Fig. 7). Different from the terminal H band, this band did not show any isotopic shift for the H_2O–D_2O substitution. When the cleaning of the electrode surface and Ar-purging of the solution were not enough, this band was observed at 2000-2020 cm^{-1} with larger intensity together with an additional band around 1800 cm^{-1}. These bands are undoubtedly assigned to the linear- and bridge-bonded CO derived from trace organic impurities in the solution [19]. The peak intensity of the linear CO band (~5×10^{-5} absorbance) is 1000-times as small as that observed on the same electrode at full CO coverage (~0.05 absorbance). Assuming the linear relationship between the band intensity and coverage [44,45], the coverage of CO is roughly estimated to be 0.001 monolayer. The CO band is not observed at lower potentials where H atoms are adsorbed at atop sites, suggesting that reduction of impurities to yield adsorbed CO or adsorption of CO is inhibited by terminal H atoms.

The integrated intensity, vibrational frequency, and width (FWHM) of the ν(Pt–H) mode observed in 0.01, 0.5, and 3 M H_2SO_4, and 1 M $HClO_4$ are plotted in Figs. 8, 9, and 10, respectively, as a function of the applied potential. The vibrational frequency was determined by curve fitting with the Gaussian function. As shown in Fig. 8, the terminal H band appears around 0.1 V and increases its intensity as the potential is made more negative in all the solutions. The data points denoted by crosses (+) in the figure were the band intensities of the terminal-H band taken from the IRA spectra by Nichols and Bewick [16] and multiplied by a factor of 8.5 for correcting the difference in sensitivity of the two surface IR techniques. The IRAS data well agree with our SEIRAS data at $E \geq 0.027$ V.

In parallel to the change in intensity, the vibrational frequency is shifted with potential at a rate ($d\nu/dE$) of about 130 cm^{-1} V^{-1} as shown in Fig. 9. The linear shift suggests that no

substantial changes occur in adsorbed state in the potential region examined. A close inspection of the figure reveals that the frequency is higher by about 3 cm^{-1} in 3 M H_2SO_4 and 1 M $HClO_4$, and lower by about 4 cm^{-1} in 0.01 M H_2SO_4, compared to the data in 0.5 M H_2SO_4. By using $d\nu/dE \sim 130$ cm^{-1} V^{-1}, the differences in the vibrational frequency (+ 3 and –4 cm^{-1}) correspond to the potential differences of +20 and –30 mV, respectively. Since the pH values of the solutions were ~ 0 for 3 M H_2SO_4 and 1 M $HClO_4$, ~ 0.5 for 0.5 M H_2SO_4, and ~ 1 for 0.01 M H_2SO_4, the difference can be correlated with the shift of RHE in the solutions (–60 mV pH^{-1}). Accordingly, the frequency data obtained in the different solutions are aligned on a single straight line if they are plotted with respect to SHE (plot not shown).

Similar potential dependent shift of vibrational frequency has been observed for a number of adsorption systems. For example, the dependence for CO on Pt is 30cm^{-1} V^{-1} for ν(C–O) [46] and –10 cm^{-1} V^{-1} for ν(Pt–CO) [47], and that for (bi)sulfate on Pt in acidic solution is ~100 cm^{-1} V^{-1} (for the band around 1200 cm^{-1}) [34]. The shift of the ν(C–O) vibration has been explained in terms of the vibrational Stark effect in the electrostatic field across the double layer [48] and/or electron backdonation from the surface to $2\pi^*$ anti-bonding orbital of CO [49, 50]. Both Stark effect and backdonation are coverage dependent [48, 51] and thus the situation is more complicated when coverage is changed with potential. Further, the change in dipole-dipole interactions between adsorbed species gives an additional shift [51]. The shifts stem from the Stark effect and dipole-dipole interaction are given by a function of the absorption coefficient of the vibration: stronger absorption bands give larger shifts [48, 51].

Compared to these adsorption systems, the shift for the ν(Pt–H) of terminal H, ~130 cm^{-1} V^{-1}, is remarkably larger. The identification and separation of the possible mechanisms are not easy even for the simplest adsorbed species. However, the contributions of the Stark effect and dipole-dipole interactions would not be so significant because the absorption

coefficient of the ν(Pt–H) band is one order of magnitude smaller than that for ν(C–O) as will be discussed later. The small contribution of the Stark effect may be supported by the independence of the $\mathrm{d}\nu/\mathrm{d}E$ of the supporting electrolyte concentration: the structure of the double-layer will be altered by the supporting electrolyte concentration. On the other hand, the small contribution of the dipole-dipole interaction is deduced from a comparison of the spectra obtained in HCl and $HClO_4$ with the same pH. The frequency of the ν(Pt–H) in HCl is 2080 cm^{-1} at –28 mV (Fig. 5) and is almost identical to that observed in $HClO_4$ at the same potential (2083 cm^{-1}, Fig. 9) despite the large difference in the band intensity (i.e. coverage). Accordingly, the potential dependence of the Pt–H bond strength is likely the main contributor for the observed peak shift. Since the frequency data in different solutions are aligned on a single straight line when they are plotted against SHE as mentioned above, the change in the Pt–H bond strength may be directly related to the shift of the Fermi level of the electrode. Although the $\mathrm{d}\nu/\mathrm{d}E$ for the ν(Pt–H) band is large, it is worth noting that the change in the Pt–H bond strength is rather small in the potential range examined: by assuming that the frequency shift stems only from the change in the Pt–H bond strength, the change in the force constant f of the ν(Pt–H) vibration is estimated to be only 2% from the observed frequency shift from 2100 to 2080 cm^{-1} ($\nu \propto \sqrt{f}$).

The band width is also potential dependent and increases as the potential is made more negative and the coverage increases (Fig. 10), suggesting the increase in lateral interaction between adsorbed terminal H atoms. The almost symmetric band shape suggests that the interaction is repulsive and terminal H atoms are distributed homogeneously over the surface to maximize their inter-atomic distance. If they were distributed randomly or form islands by attractive interaction, the band shape should be asymmetric [51].

3.3.2 Kinetic analysis of the spectrum of terminal H.

The Tafel slope of 30 mV/decade observed in Fig. 2 is explained by assuming that the

discharge of H_3O^+ to yield the intermediate H(a) and the corresponding ionization of H(a) back to H_3O^+, eq. (1), is in quasi-equilibrium, and that the following Tafel step is rate determining. We have the relation between the activity of the intermediate $a_{H(a)}$ and overpotential η (=E – E_{eq}) as

$$(a_{H(a)} / a_{H(a),eq}) = \exp(-F\eta / RT), \quad (4)$$

where $a_{H(a),eq}$ is the activity at the equilibrium potential E_{eq}. When experiments are conducted under an inert atmosphere where the backward reaction (i.e. HOR) can be neglected, the rate of recombination of two adsorbed H atoms is proportional to the square of $a_{H(a)}$ for the Volmer-Tafel mechanism and thus the hydrogen evolution current i is given by

$$i = 2Fk\left(a_{H(a)}\right)^2, \quad (5)$$

where k is the rate constant. By taking logarithm of the equation, we have

$$\log i = \log\left(2Fka_{H(a),eq}^2\right) - \frac{2}{2.303}\frac{F}{RT}\eta. \quad (6)$$

The slope of $2F/2.303RT$ = $(29.6\ mV)^{-1}$ (at 25 ºC) is what we observed in the Tafel plots (Fig. 2).

In the framework of the Volmer-Tafel mechanism, we derive the relation between i and the band intensity of the hydrogen intermediate $A_{H(a)}$ by assuming that $A_{H(a)}$ is proportional to coverage $\theta_{H(a)}$. Although the proportionality between band intensity and coverage is not guaranteed for some adsorption systems (for example, CO adsorbed on Rh(111) in UHV [52]), it is a reasonable assumption in electrochemical environment [44,45]. A support is obtained from the linear potential dependence of $\theta_{H(a)}$ on a polycrystalline Pt surface at $-1 < E < 0$ V determined by impedance spectroscopy [53]. In parallel to the coverage data, the band intensity is proportional to the applied potential at $E < 0$ V (Fig. 8).

Since $a_{H(a)}$ approximately equals to $\theta_{H(a)}$ at very low coverage, $a_{H(a)}$ is written as

$$a_{\mathrm{H(a)}} = \theta_{\mathrm{H(a)}} = A_{\mathrm{H(a)}} \Big/ A^{\circ}_{\mathrm{H(a)}} \,, \tag{7}$$

where $A^{\circ}_{\mathrm{H(a)}}$ is the band intensity at $\theta_{\mathrm{H(a)}} = 1$. From Eqs. 4, 5, and 7, we have

$$\log A_{\mathrm{H(a)}} = \log A^{\circ}_{\mathrm{H(a)}} + \log a_{\mathrm{H(a),eq}} - \frac{1}{2.303}\frac{F}{RT}\eta \tag{8}$$

and

$$\log i = \log\left[2Fka^{2}_{\mathrm{H(a),eq}} \Big/ \left(A^{\circ}_{\mathrm{H(a)}}\right)^{2}\right] + 2\log A_{\mathrm{H(a)}} \,. \tag{9}$$

The linear relations between log $A_{\mathrm{H(a)}}$ and η and between log i and log $A_{\mathrm{H(a)}}$ can be found for the ν(Pt–H) band of terminal H at positive potentials (i.e. the low current density region), as shown in Figs. 11 and 12. The slope of the log $A_{\mathrm{H(a)}}$ versus E plot (Fig. 11) is approximately (60 mV)$^{-1}$ (= F/2.303RT) and that of the log i versus log $A_{\mathrm{H(a)}}$ plot (Fig. 12) is 2 in the potential range of 0.02 < E < 0.1 V, as is expected from Eqs. 8 and 9. The results clearly demonstrate that terminal H is the reaction intermediate. Although Eq. 8 holds also for the Volmer-Heyrovsky mechanism with the latter being rate determining [1,2], the slope 2 of the log i versus log $A_{\mathrm{H(a)}}$ plot (i.e. $i \propto \left(\theta_{\mathrm{H(a)}}\right)^{2}$) definitely confirms the Tafel step being rate determining.

The band intensity data deviate from the expected straight lines at low potentials (i.e. for high current densities), while the Tafel slope is constant at 30 mV/decade over the potential range examined (Fig. 2). In our previous publication [22], the deviation was tentatively explained in terms of supersaturation effect of H_2 at the interface, which can give an apparent Tafel slope around 30 mV/decade independent of the mechanism [3,4,15,54,55]. However, it should be noted that the assumption of $a_{\mathrm{H(a)}} = \theta_{\mathrm{H(a)}}$ holds only at low coverage. At higher coverage, $a_{\mathrm{H(a)}}$ should be represented by a more general adsorption isotherm. Here we express the activity with the Frumkin isotherm

$$a_{\mathrm{H(a)}} = \left[\theta_{\mathrm{H(a)}} / \left(1 - \theta_{\mathrm{H(a)}}\right)\right] \exp\left(g\theta_{\mathrm{H(a)}}\right), \tag{10}$$

where the dimensionless parameter g represents the lateral interaction between adsorbed H atoms (repulsive for $g > 0$ and attractive for $g < 0$). For $g = 0$, the Frumkin isotherm is reduced to the Langmuir isotherm. The adsorption of H_{upd} is known to follow the Frumkin isotherm [5,6,8,56-58] and the isotherm is used also to describe the adsorption of H_{opd} [5]. We show below that the deviation of the IR intensity data from the linear relations at high current densities can be removed by the use of the Frumkin isotherm.

The band intensity at saturation $A^{\circ}_{H(a)}$ required for calculating $\theta_{H(a)}$ from the band intensity data could not be determined in the present study due to the limited potential range (saturation of the band intensity is not seen in Fig. 8). Although a $\theta_{H(a)}$ versus η plot for a polycrystalline Pt electrode determined by ac impedance in 0.5 M H_2SO_4 has been reported in the literature [53], the data was obtained unfortunately with an unactivated (i.e., contaminated) electrode. Therefore, we tentatively use the $\theta_{H(a)}$ versus potential plots for Pt(111), (110), and (100) in 0.5 M H_2SO_4 [15] by assuming that our polycrystalline electrode surface is a mixture of the single-crystal domains. Specifically, the coverages we used for the data analysis were 0.3 (for (100)), 0.55 (for (110)), and 0.65 (for (111)) at –50 mV. From the observed integrated band intensity of 0.081 cm^{-1} at –50 mV (Fig. 8), $A^{\circ}_{H(a)}$ is calculated to be 0.27, 0.147, and 0.125 cm^{-1}, respectively. These values are smaller than that for linear CO (~1 cm^{-1} measured with un-polarized radiation) and are reasonable because CO adsorbed on Pt is known to be an exceptionally strong IR absorber and the dynamic dipole moment associated with Pt–H vibration should be small [9]. We adjusted g value for each $A^{\circ}_{H(a)}$ value so that the slope of the log i versus log $a_{H(a)}$ plot generate a straight line with a slope 2 over the potential range examined (i.e. by assuming the Tafel step being rate determining). The results for the data obtained in 0.5 M H_2SO_4 are shown in Fig. 13a. The best-fit g values were 1.9, 2.5 and 6.2 for $A^{\circ}_{H(a)}$ = 0.125, 0.147, and 0.27 cm^{-1}, respectively. It is worth noting that the linear

relation between log i and log $a_{H(a)}$ is realized only for g > 0 (repulsive interaction), which is consistent with the homogeneous broadening of the ν(Pt–H) vibration of terminal H (Fig. 7). Fig. 13b represents the potential dependence of log $a_{H(a)}$ calculated with the parameters. The reasonable linearly is observed with the expected slope of $(60\ \text{mV})^{-1}$ for the all $A^{\circ}_{H(a)}$ values. A close inspection of Fig. 13a reveals, however, that the linearity between log i and log $a_{H(a)}$ is better for smaller g values (the plot for g = 6.2 appears to be fitted more reasonably by a curve rather than the straight line), suggesting that the true g value is closer to 1.9 rather than 6.2. The estimated g value is close to or smaller than those for H_{upd} on single-crystal Pt surfaces; 2-4 for (100) and (110) [56,57] and 11-18 for (111) [14,56-58].

To check the validity of the approach mentioned above, we took another approach in which the band intensity data is directly fitted to the electrochemical Frumkin isotherm derived from Eqs. 4 and 10

$$a_{H(a),eq}\exp(-F\eta/RT) = \left[\theta_{H(a)}/(1-\theta_{H(a)})\right]\exp(g\theta_{H(a)}) \qquad (11)$$

without assuming $A^{\circ}_{H(a)}$. Since $a_{H(a),\ eq}$ and E_{eq} are also unknown, these quantities (more exactly, ln $a_{H(a),\ eq}$ + $(F/RT)E_{eq}$) were also treated as the adjusting parameters. The best fit to the data in 0.5 and 3 M H_2SO_4 was obtained for $A^{\circ}_{H(a)}$ = 0.10 cm^{-1} and g = 1.34 as shown by the curve in Fig. 14. The parameter values are close to that deduced by the first approach, and the linear relations between log i and log $a_{H(a)}$ and between log $a_{H(a)}$ and E were realized with the proportional constants of 1.9 and $(56\ \text{mV})^{-1}$, respectively (plots not shown). It should be emphasized that the second approach gives the relations expected for the Volmer-Tafel mechanism without assuming this reaction mechanism.

Although a unique set of g and $A^{\circ}_{H(a)}$ could not be determined definitely due to the limited potential range and the scatter of the experimental data, the following three issues can be concluded safely: (i) terminal H atom that gives the ν(Pt–H) band at 2080-2100 cm^{-1} is the

reaction intermediate in HER, (ii) the recombination of two terminal H atoms (Tafel step) is the rate-determining step in HER, and (iii) lateral repulsive interaction exists between adsorbed H atoms. The repulsive interaction increases the activity of terminal H atoms (Eq. 9) and can facilitate their recombination yielding H_2.

We do not know how a pair of terminal H atoms separated by 0.279 nm (the nearest neighbor Pt–Pt distance) are combined to form a H_2 molecule with a H–H distance of 0.074 nm. However, it could be imagined that the recombination occurs through a transition state like dihydride, H_2–Pt. Peremans and Tadjeddine [20,21] assigned the SFG peak at 1770 cm^{-1} to a dihydride and claimed that the dihydride is a reactive intermediate in HER. In contrast to the SFG experiment, we did not observe the corresponding vibration in the present experiments despite the very high sensitivity of SEIRAS. Although we observed a very weak band at ~ 1800 cm^{-1} when the cleaning of the electrode surface was not enough, this band is ascribed to bridge CO from the independence of the solvent (H_2O and D_2O). Since SFG-active modes are IR-active, the discrepancy cannot be ascribed to the difference in the selection rules in SFG and IR. Although further detailed studies are required, it may be worth mentioning again that Pt surface is easily contaminated with CO even if ultrapure water and chemicals are used [19,53].

3.4. Role of H_{upd} in HER

The SEIRAS study conclusively demonstrated that the reaction intermediate in HER on polycrystalline Pt is terminal H (H_{opd} in the thermodynamic notation). However, Markovic et al. [6,14] suggested that H_{opd} plays some role in HER and HOR. Since the upd of H is sensitive to the crystallographic orientation of the Pt surface [5,8,14,15], this suggestion can reasonably explain the structural dependence of HER and HOR kinetics. Although the structural dependence is out of scope in the present study, we would like to discuss below the role of H_{upd} in HER in the context of aforementioned results with the aid of rich information

from surface science in UHV [9].

Hydrogen atom has a strong tendency to be adsorbed at hollow sites [9] and thus full or nearly full occupation of hollow sites by H_{upd} is of primary importance for opd at atop sites. In addition, the repulsive interaction between H_{upd} atoms [4-6,8,14,56-58] lowers the heat of adsorption [8,9,14] and may facilitate the adsorption of H_{opd} atoms at atop sites. First principle calculations predict that the adsorption energy at atop sites becomes lower as the coverage increases [36]. Considering the extremely fast surface diffusion of adsorbed H atoms [9], however, the distinction of H_{upd} and H_{opd} would not be realistic and rather it appears more reasonable to suggest that adsorbed H atoms dynamically change their adsorption sites between hollow and atop sites.

The lowering of the heat of adsorption can be related to the change in electronic structure of Pt that can be monitored through the change in work function (in UHV) [9] and reflectivity in the visible, near-IR, and IR regions (in electrochemical environment) [17,29]. The H-induced shift of work function is about –100 meV for Pt(111) and –500 meV for Pt(110) at full coverage (at hollow sites) [9]. Since the potential dependence of the terminal H vibration ($d\nu/dE \sim 130\ cm^{-1}\ V^{-1}$) is related mainly to the shift of the Fermi level as mentioned before, the H-induced work function shift can lower the frequency by 13–65 cm^{-1}. Accordingly, the vibrational frequency of terminal H is predicted to be structure dependent. Unfortunately, the existing IR data on Pt single-crystal surfaces [16-18,20,21] are controversial each other and thus careful reinvestigation is desirable to conclude the discussion in this section. Nevertheless, it should be noted that, even if a large surface structure dependence were observed in the Pt–H vibration (say a frequency difference by 100 cm^{-1}), the structure dependence of the Pt–H bond strength itself is only ~10% and is not significant to explain the structural dependence of HER and HOR kinetics.

4. Conclusion

ATR-SEIRAS enabled us to study hydrogen evolution reaction (HER) on a polycrystalline Pt electrode surface without the interference from evolved H_2 gas. A band characteristic to H atoms adsorbed at atop sites (terminal H atoms) appears at 2095 cm^{-1} at about 0.1 V and increases its intensity at less positive potentials down to –60 mV (the lowest potential limited by ohmic drop) accompanying by the frequency shift at a rate of ~130 cm^{-1} V^{-1} and broadening of the band width. The spectral feature at potentials more positive than +27 mV was identical to that observed in the earlier IRAS study by Nichols and Bewick [16,17]. The very high sensitivity of SEIRAS, 28 times higher than IRAS for p-polarization and 8.5 times for unpolarized radiation, allowed the quantitative comparison of the band intensity data with the kinetics of HER (Tafel plot). The analysis demonstrated that terminal H atom is the reaction intermediate in HER and that HER occurs via the Volmer-Tafel mechanism with the latter being rate determining. It also showed that the adsorption of terminal H is represented by the Frumkin isotherm with repulsive lateral interaction between adsorbed H atoms. The repulsive interaction was deduced also from the symmetric shape of the terminal H band. Despite the high sensitivity of SEIRAS, however, no signals of underpotentially deposited H atoms that are speculated to be located at hollow sites were detected.

Acknowledgements

This work was supported by the Ministry of Education, Culture, Sports, Science and Technology of Japan (Grant-in-Aid for Basic Research No. 18350038 and for Scientific Research on Priority Areas 417) and Japan Science and Technology Agency.

References

[1] R. Parsons, Trans. Faraday Soc. 34 (1958) 1053.

[2] P. Delahay, Double Layer and Electrode Kinetics, Interscience, New York, 1965.

[3] A.J. Appleby, H. Kita, M. Chemila, G. Bronoel, in: A. J. Bard (Ed.), Encyclopedia of Electrochemistry of the Elements, vol. IX-A, Marcel Dekker, New York, 1982, Chapter IX.

[4] B.E. Conway, in: A. Wieckowski (Ed.), Interfacial electrochemistry: theory, experiment, and applications, Marcel Dekker, New York, 1999, p. 131.

[5] B.E. Conway, G. Jerkiewicz, Electrochim. Acta 45 (2000) 4075.

[6] N.M. Marković, P.N. Ross, Surf. Sci. Rept. 45 (2002) 117.

[7] H. Kita, J. Molecular Cat. A: Chemical 199 (2003) 161.

[8] G. Jerkiewicz, Prog. Surf. Sci. 57 (1998) 137.

[9] K. Christmann, Surf. Sci. Rept. 9 (1988) 1 and references therein.

[10] S. Schuldiner, M. Rosen, D.R. Flinn, J. Elechrochem. Soc. 117 (1970) 1251.

[11] K. Seto, A. Ianelli, B. Love, J. Lipkowski, J. Electroanal. Chem. 226 (1987) 351.

[12] H. Kita, S. Ye, Y. Gao, J. Electroanal. Chem. 334 (1992) 351.

[13] R. Gómez, A. Fernández-Vega, J.M. Felui, A. Aldaz, J. Phys. Chem. 97 (1993) 4769.

[14] N.M. Marković, B.N. Grgur, P.N. Loss, J. Phys. Chem. B 101 (1997) 5405.

[15] J. Barber, S. Morin, B.E. Conway, J. Electroanal. Chem. 446 (1998) 125.

[16] R.J. Nichols, A. Bewick, J. Electroanal. Chem 243 (1988) 445.

[17] R.J. Nichols, in: J. Lipkowski, P. N. Ross (Eds.), Adsorption of molecules at metal electrodes, VCH, New York, 1992, p. 347.

[18] H. Ogasawara, M. Ito, Chem. Phys. Lett. 221 (1994) 213.

[19] N. Nanbu, F. Kitamura, T. Ohsaka, K. Tokuda, J. Electroanal. Chem. 485 (2000) 128.

[20] A. Peremans, A. Tadjeddine, Phys. Rev. Lett. 73 (1994) 3010.

[21] A. Tadjeddine, A. Peremans, J. Electroanal. Chem. 409 (1996) 115.

[22] K. Kunimatsu, T. Senzaki, M. Tsushima, M. Osawa, Chem. Phys. Lett. 401 (2005) 451.

[23] M. Osawa, Bull. Chem. Soc. Jpn. 70 (1997) 2861.

[24] M. Osawa, Top. Appl. Phys. 81 (2001) 163.

[25] K. Kunimatsu, H. Uchida, M. Osawa, M. Watanabe, J. Electroanal. Chem. 587 (2006) 299.

[26] M. Osawa, K. Ataka, K. Yoshii, T. Yotsuyanagi, J. Electron Spectrosc. Relat. Phenom. 64/65 (1993) 371.

[27] K. Ataka, T. Yotsuyanagi, M. Osawa, J. Phys. Chem. 100 (1996) 10664.

[28] A. Miki, S. Ye, M. Osawa, Chem. Commun. (2002) 1500.

[29] A. Miki, S. Ye, T. Senzaki, M. Osawa, J. Electroanal. Chem. 563 (2004) 23.

[30] A.J. Bard, L.R. Faulkner, Electrochemical Methods, 2nd Ed., Wiley, New York, 2001. p. 645.

[31] H. Angerstein-Kozlowska, B.E. Conway, W.B.A. Sharp, J. Electroanal. Chem. 43 (1973) 9.

[32] M. Osawa, K. Ataka, K. Yoshii, Y. Nishikawa, Appl. Spectrosc. 47 (1993) 1497.

[33] K. Kunimatsu, M. Samant, H. Seki, M.R. Philpott, J. Electroanal. Chem. 243 (1988) 203.

[34] K. Kunimatsu, M.G. Samant, H. Seki, J. Electroanal. Chem. 258 (1989) 163.

[35] K. Ataka, M. Osawa, Langmuir 14 (1998) 951.

[36] S.C. Badescu, K. Jacobi, Y. Wang, K. Bedurftig, G. Ertl, P. Salo, T. Ala-Nissila, S.C. Ying, Phys. Rev. B 68 (2003) 205401.

[37] J.E. Reutt, Y.J. Chabal, S.B. Cristman, J. Electron Spectrosc. Relt. Phenom. 44 (1987)

325.

[38] J.O'M. Bockris, M. Gamboa-Aldeco, M. Szklarczyk, J. Electroanal. Chem. 339 (1992) 355.

[39] K. Nakamoto, Infrared and Raman Spectra of Inorganic and Coordination Compounds, 4th Ed., John Wiley & Sons, New York, 1986, p. 116 and references therein.

[40] W.-B. Cai, L.-J. Wan, H. Noda, Y. Hibino, K. Ataka, M. Osawa, Langmuir 14 (1998) 6992.

[41] H. Miyake, M. Osawa, T. Okada, Chem. Phys. Lett. 428 (2006) 451.

[42] H. Miyake, T. Uchida, M. Osawa, to be published.

[43] M. Osawa, M. Kuramitsu, A. Hatta, W. Suëtaka, H. Seki, Surf. Sci. Lett. 175 (1986) L787.

[44] K. Kunimatsu, J. Electroanal. Chem. 213 (1986) 149.

[45] L.-W.H. Leung, A. Wieckwski, M.J. Weaver, J. Phy. Chem. 92 (1988) 6985.

[46] K. Kunimatsu, H. Seki, W.G. Golden, J.G. Gordn, M.R. Philpott, Surf. Sci. 158 (1985) 596.

[47] S. Zou, M.J. Weaver, J. Phys. Chem. 100 (1996) 4237.

[48] D.K. Lambert, Electrochim. Acta 41 (1995) 623.

[49] N.K. Ray, A.B. Anderson, J. Chem. Phys. 86 (1982) 4851.

[50] S. Holloway, J.K. Norskov, J. Electroanal. Chem. 161 (1984) 193.

[51] F.M. Hoffmann, Surf. Sci. Rept. 3 (1983) 107.

[51] H. Pfnür, A. Menzel, F.M. Hoffmann, A. Ortega, A.M. Bradshaw, Surf. Sci. 93 (1980) 431.

[53] L. Bai, D.A. Harrington, B.E. Conway, Electrochim. Acta 32 (1987) 1713.

[54] B.E. Conway, L. Bai, J. Electroanal. Chem. 198 (1986) 149.

[55] M. Briter, in: E. Yeager (Ed.), Transactions of the Symposium on Electrode Processes,

Wiley, New York, 1961, p. 307.

[56] A. Zolfaghari, G. Jerkiewicz, J. Electroanal. Chem. 467 (1999) 177.

[57] A. Lasia, J. Electroanal. Chem. 562 (2004) 23.

[58] R. Gómez, J.M. Orts, B. Alvarez-Ruiz, J.M. Feliu, J. Phy. Chem. B 108 (2004) 228.

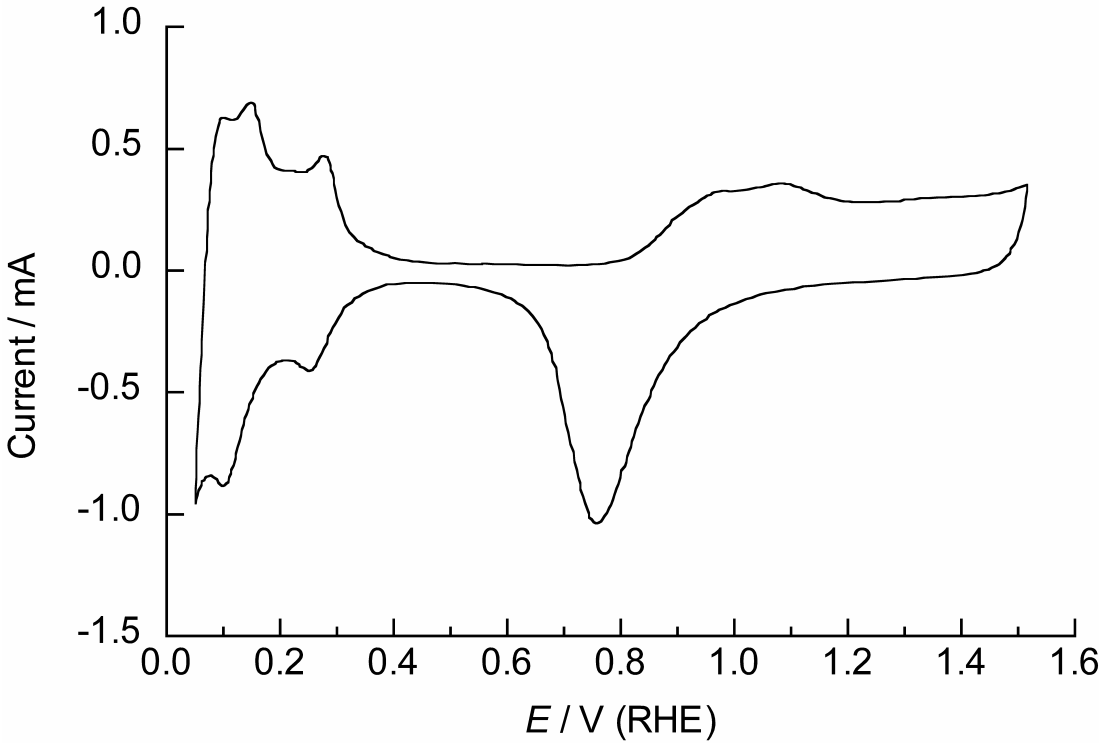

Fig. 1. Cyclic voltammogram for a chemically deposited Pt film electrode in 0.5 M H_2SO_4 at 50mV s^{-1}.

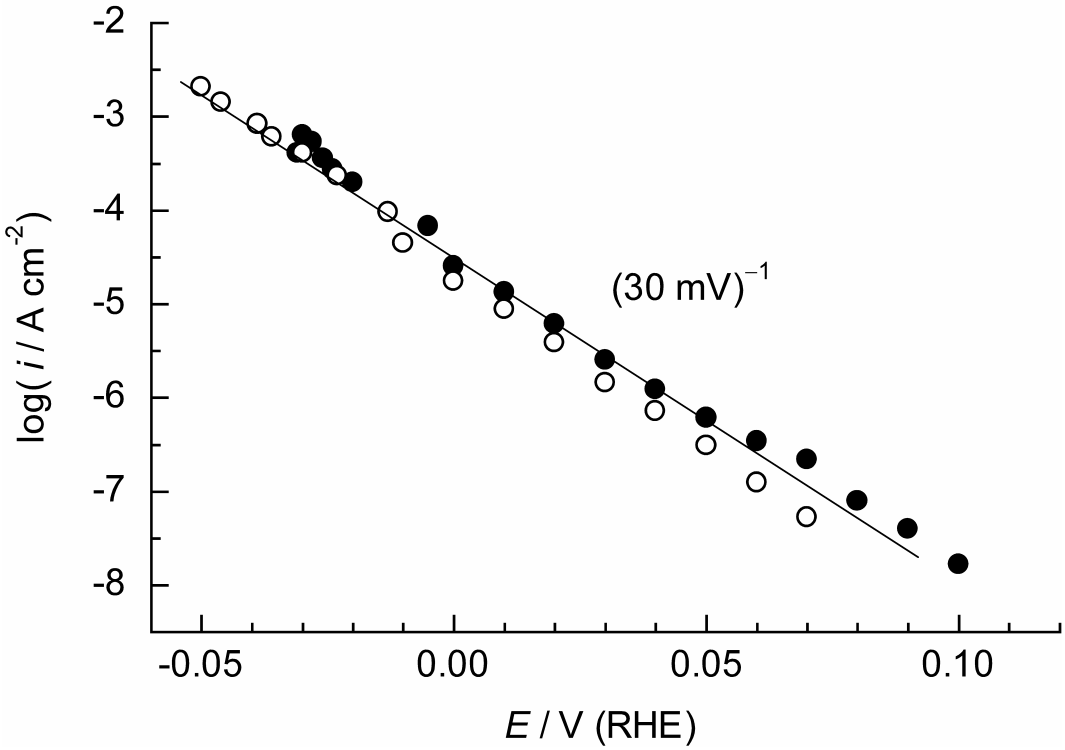

Fig. 2. Tafel plots for the chemically deposited thin Pt film electrode in 0.5 M H_2SO_4 (●) and 1 M $HClO_4$ (○).

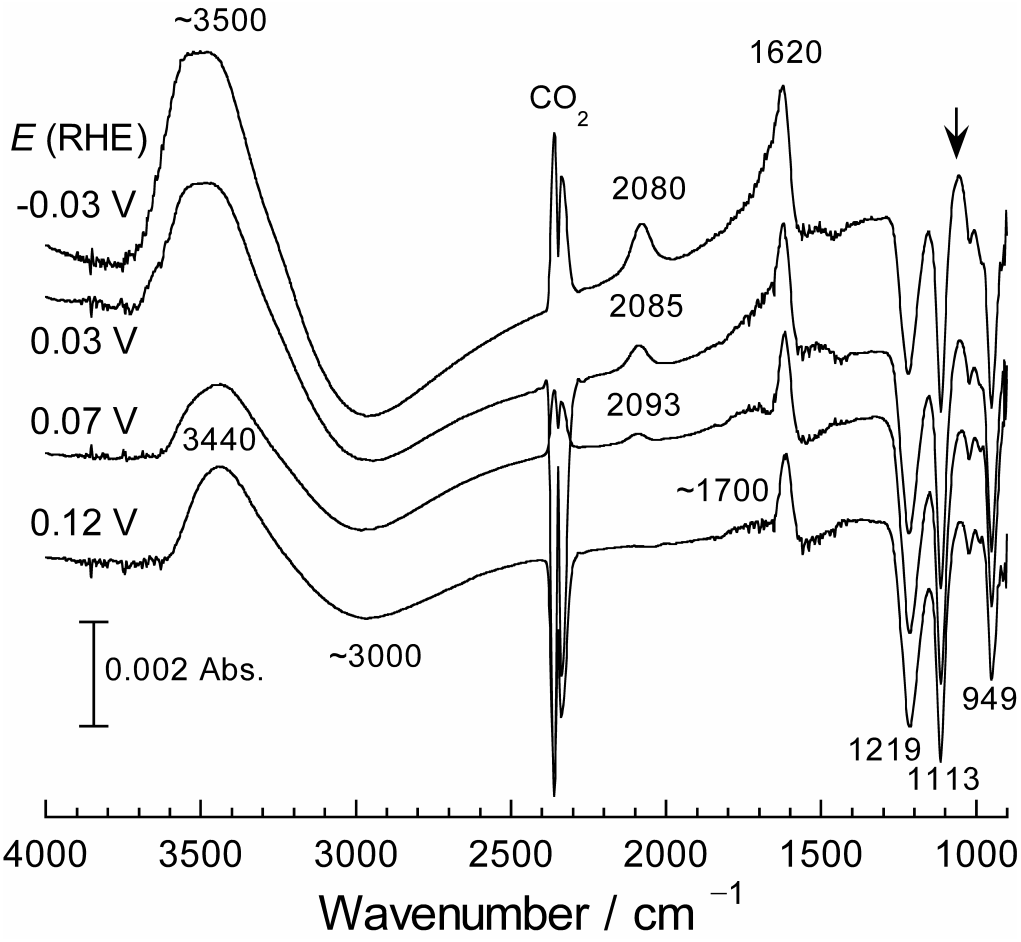

Fig. 3. SEIRA spectra of the Pt electrode surface observed in 0.5 M H_2SO_4 at the sample potentials shown in the figure with respect to the reference potential of 0.6 V. The arrow indicates the presence of a band that increases in intensity as the potential *E* is made more negative..

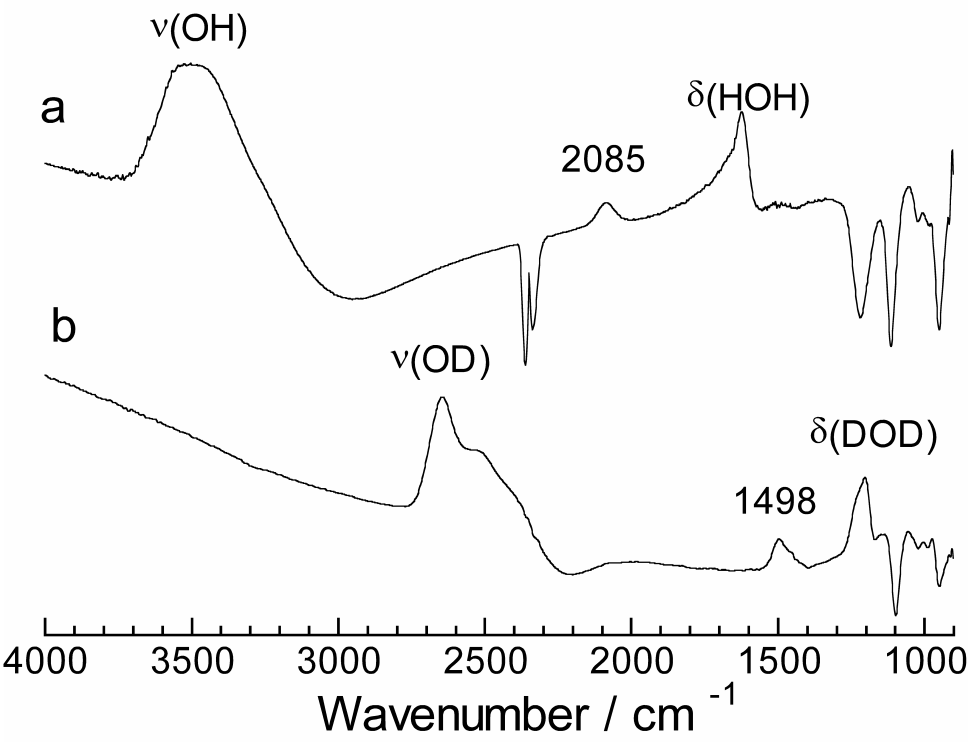

Fig. 4. SEIRA spectra of the Pt electrode surface observed in H_2O (a) and D_2O (b) solutions of 0.5 M H_2SO_4 at 0 V with respect to 0.6 and 0.2 V, respectively. The potentials are against RHE for the former and RDE for the latter.

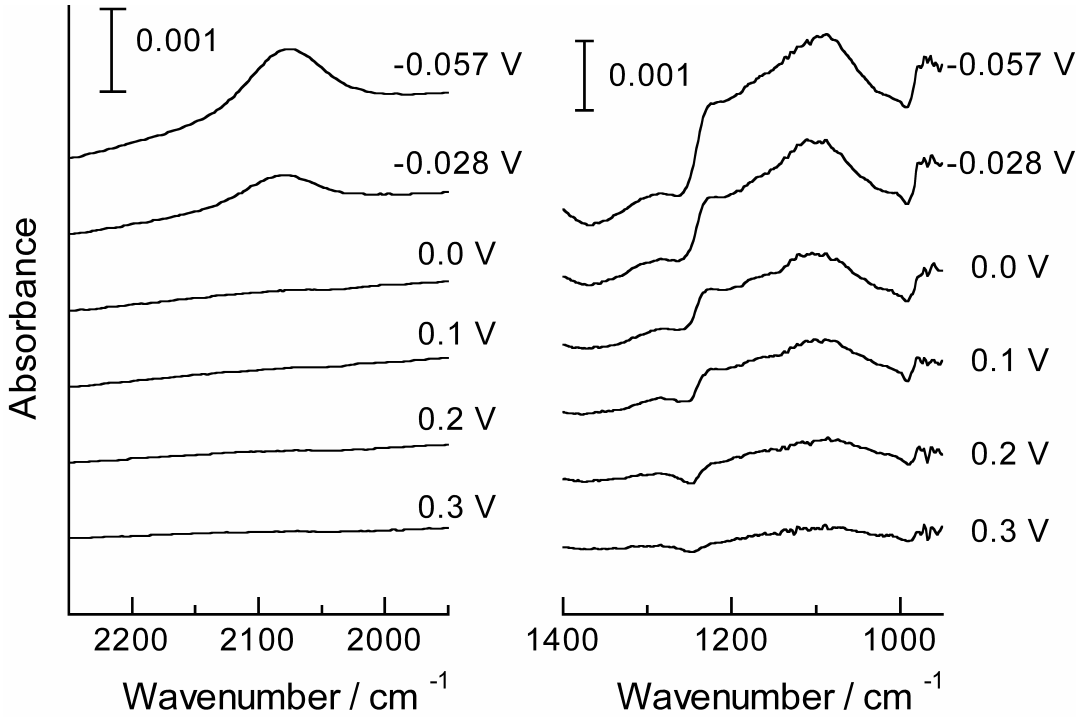

Fig. 5. SEIRA spectra of the Pt electrode surface observed in 1 M HCl at the sample potentials shown in the figure with respect to the reference potential of 0.4 V.

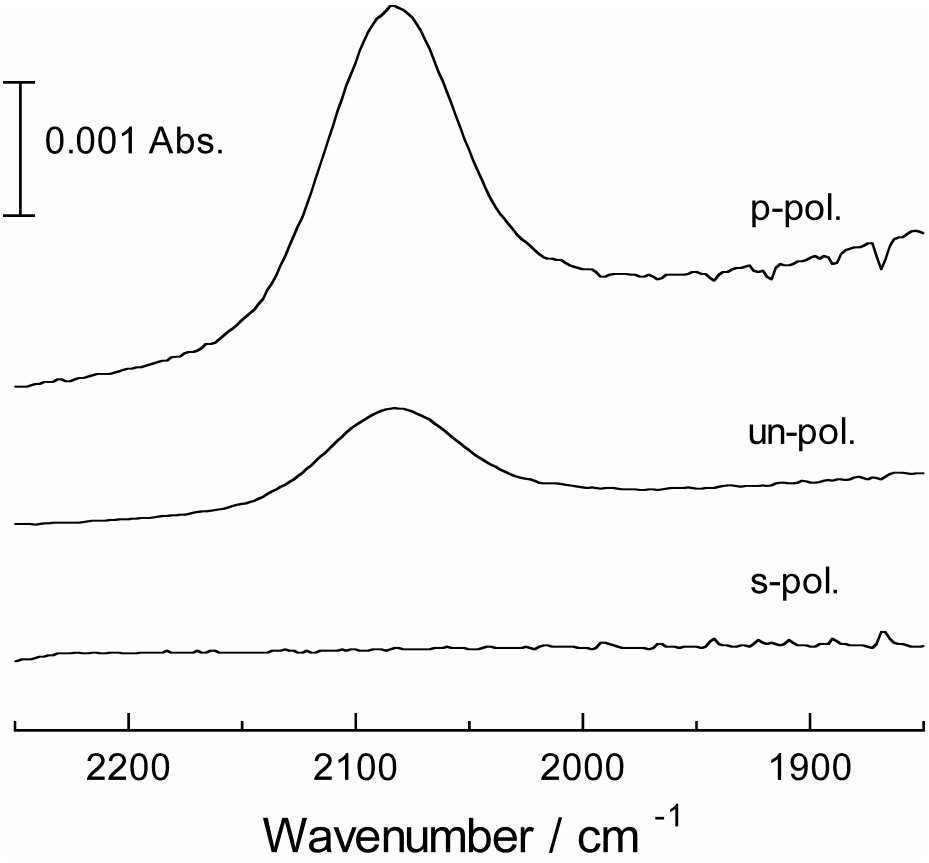

Fig. 6. Dependence of the incident IR polarization on the SEIRA spectra observed at 0.0 V in 3 M H_2SO_4.

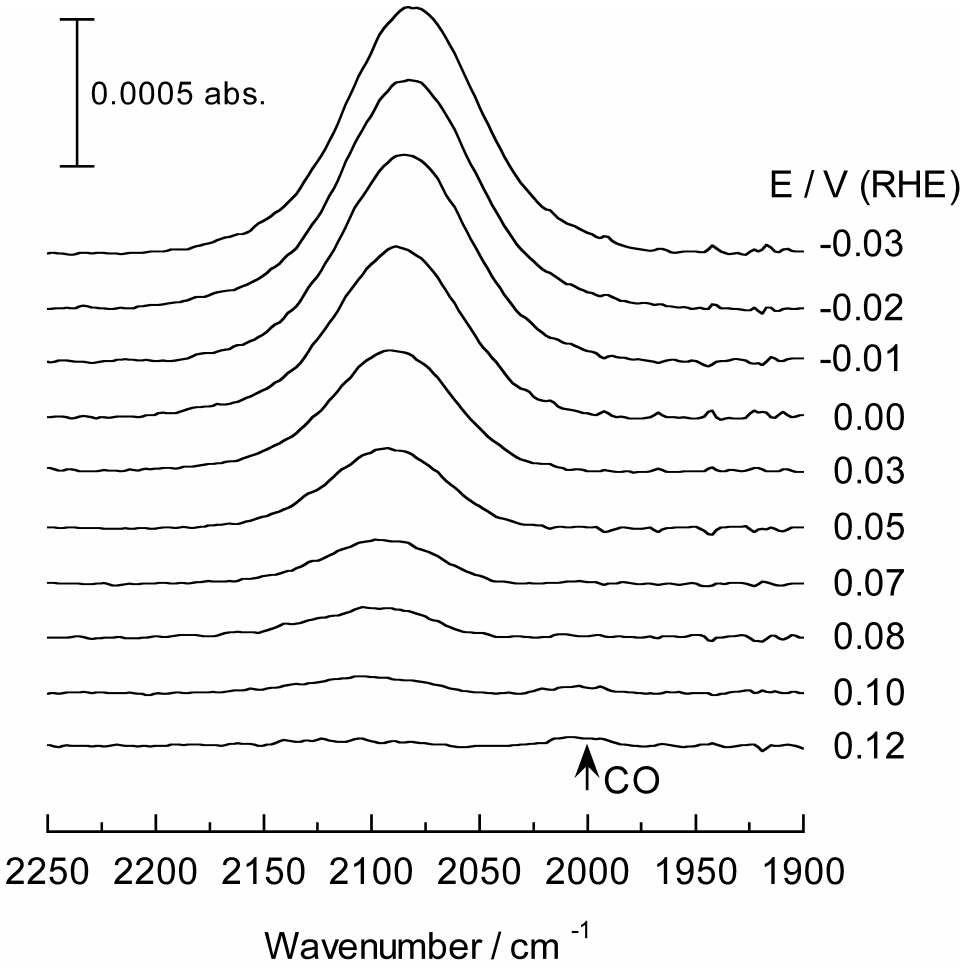

Fig. 7. Potential dependence of the SEIRA spectrum of terminal H observed in 0.5 M H_2SO_4. The spectra were baseline corrected and offset for clarity.

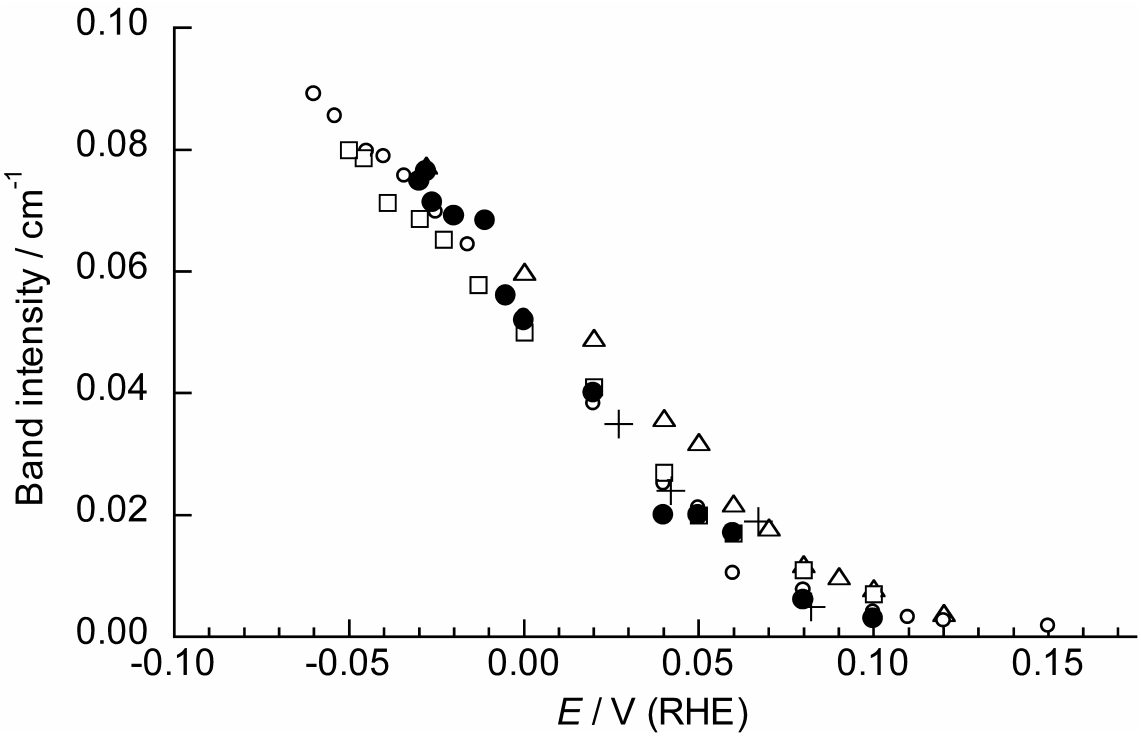

Fig. 8. Potential dependence of the integrated band intensity of terminal H observed in 0.01M (△), 0.5 M (●), and 3 M H_2SO_4 (○), and 1 M $HClO_4$ (□). The data points shown by + were taken from the reference [16] and multiplied by a factor of 8.5 to compensate the difference in sensitivity between SEIRAS and IRAS.

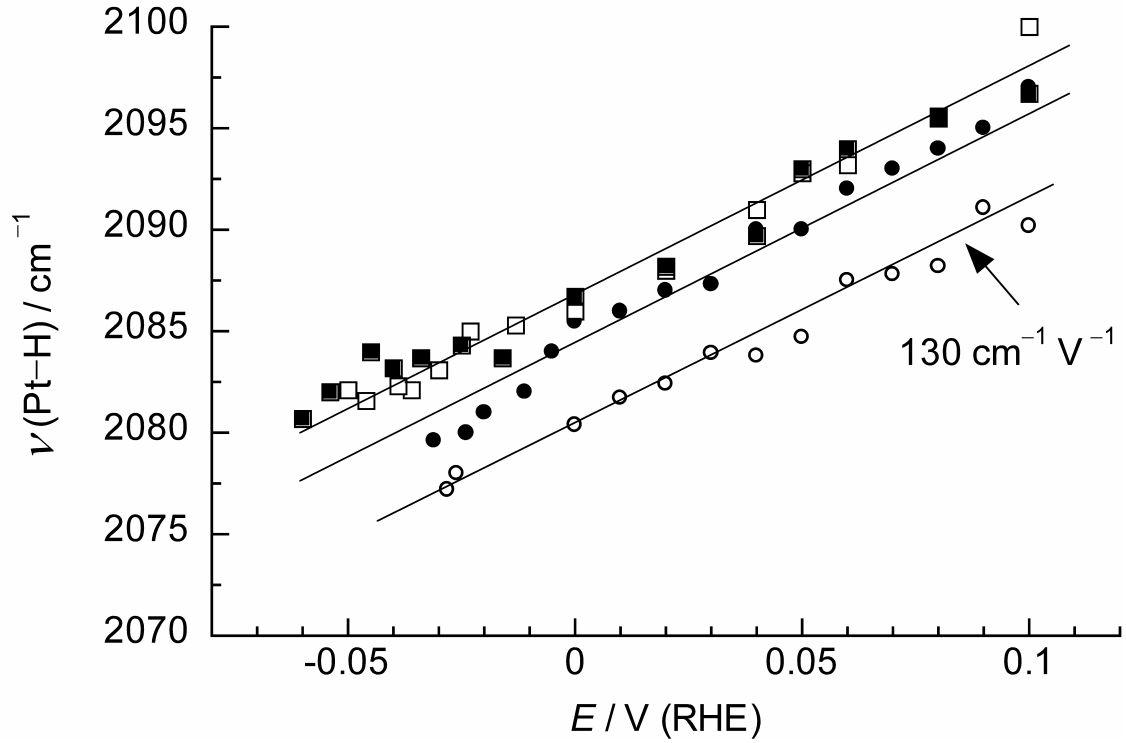

Fig. 9. Potential dependence of the vibrational frequency of terminal H observed in 0.01 (○), 0.5 (●), and 3 M (■) H_2SO_4, and 1 M $HClO_4$ (□).

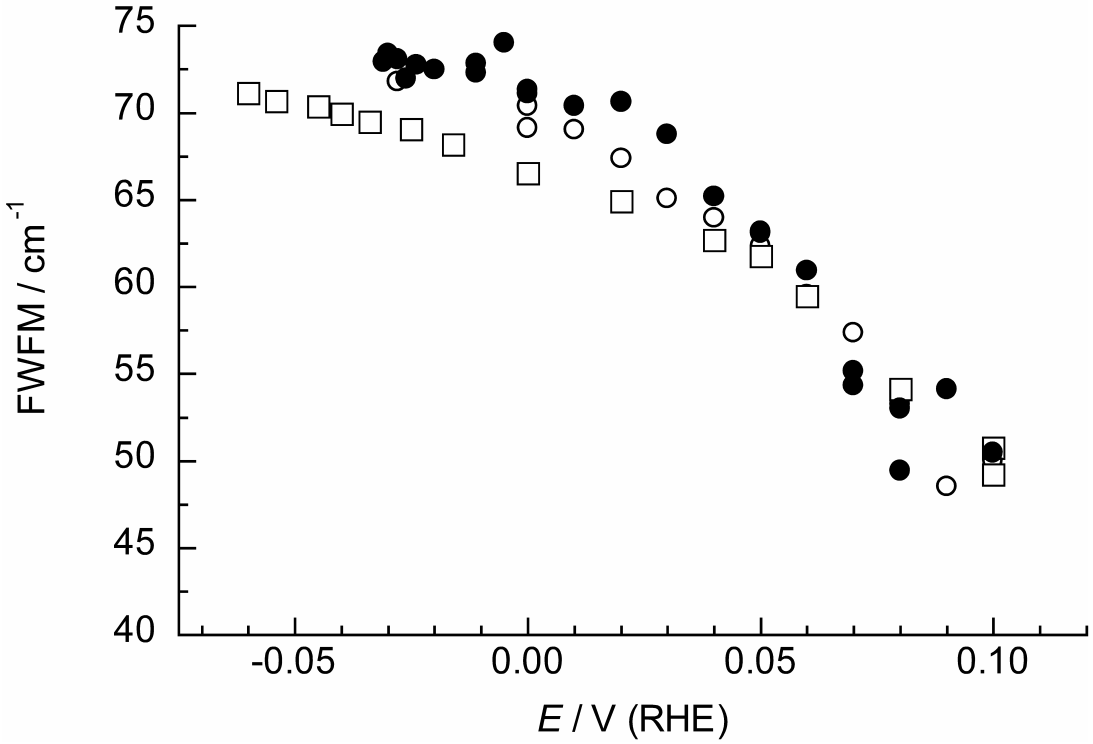

Fig. 10. Potential dependence of the band width (FWHM) of terminal H observed in 0.01 (○), 0.5 (●), and 3 M (□) H_2SO_4.

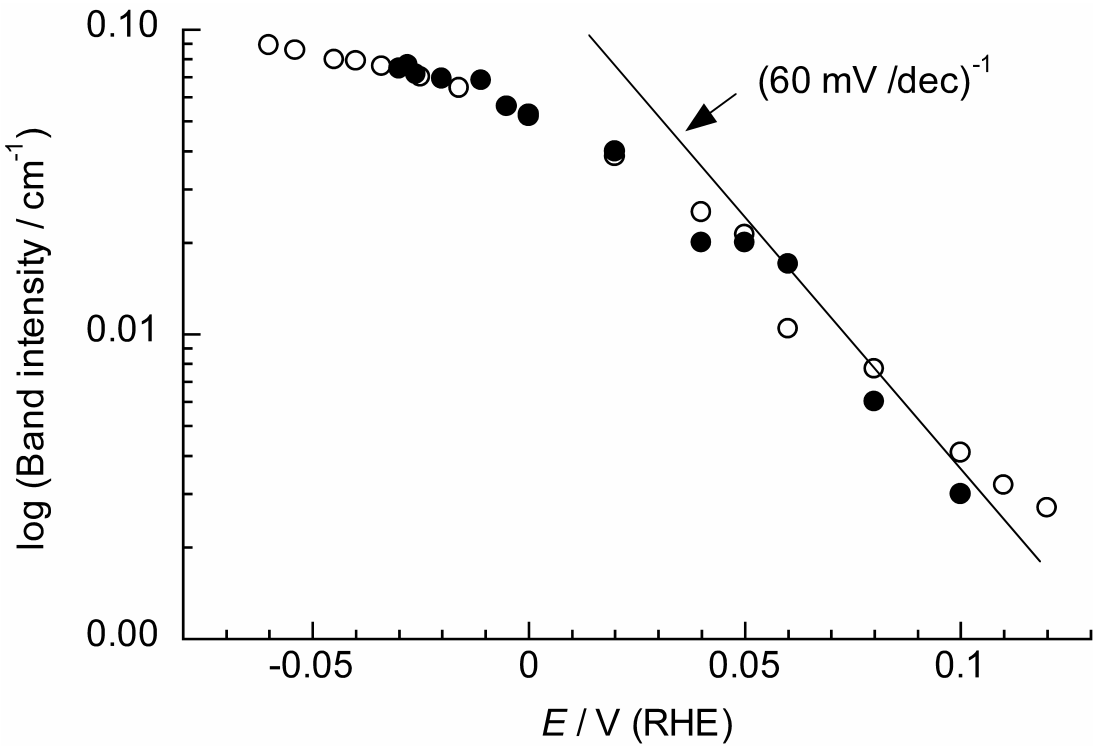

Fig. 11. Logarithmic plot of the band intensity of terminal H against the applied potential *E* observed in 0.5 (●) and 3 M (○) H_2SO_4.

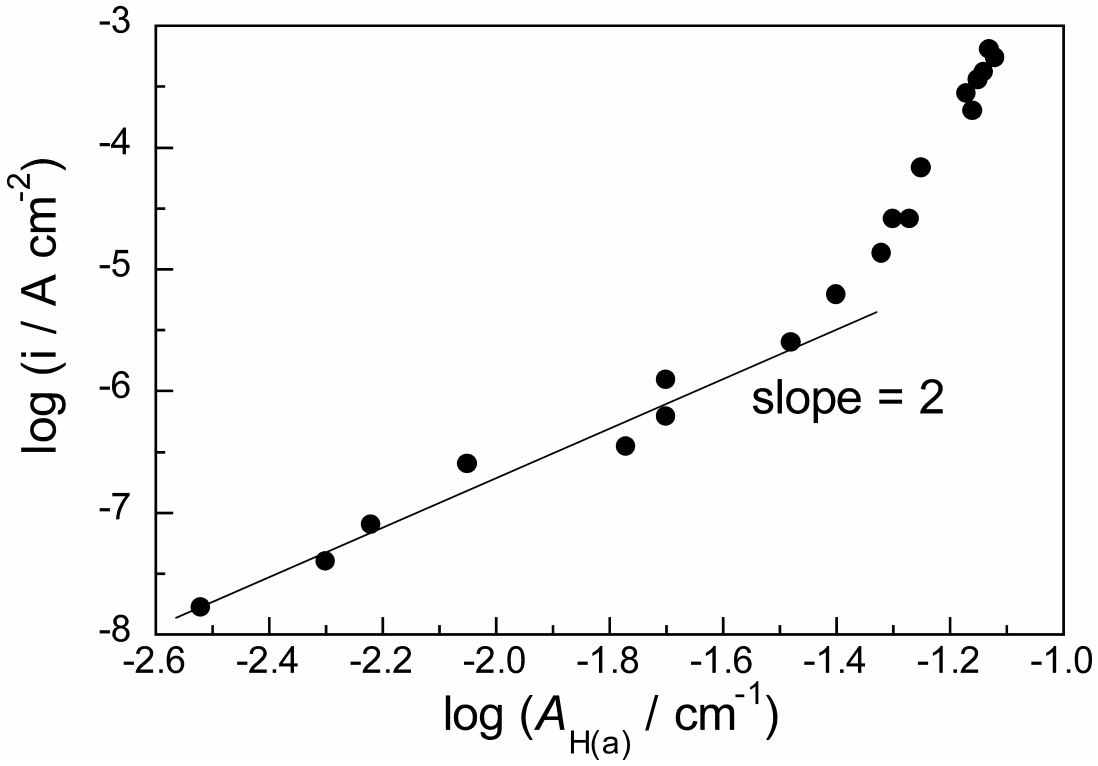

Fig. 12. Log-log plot of the current density and the infrared band intensity of terminal H ($A_{H(a)}$) observed in 0.5 M H_2SO_4.

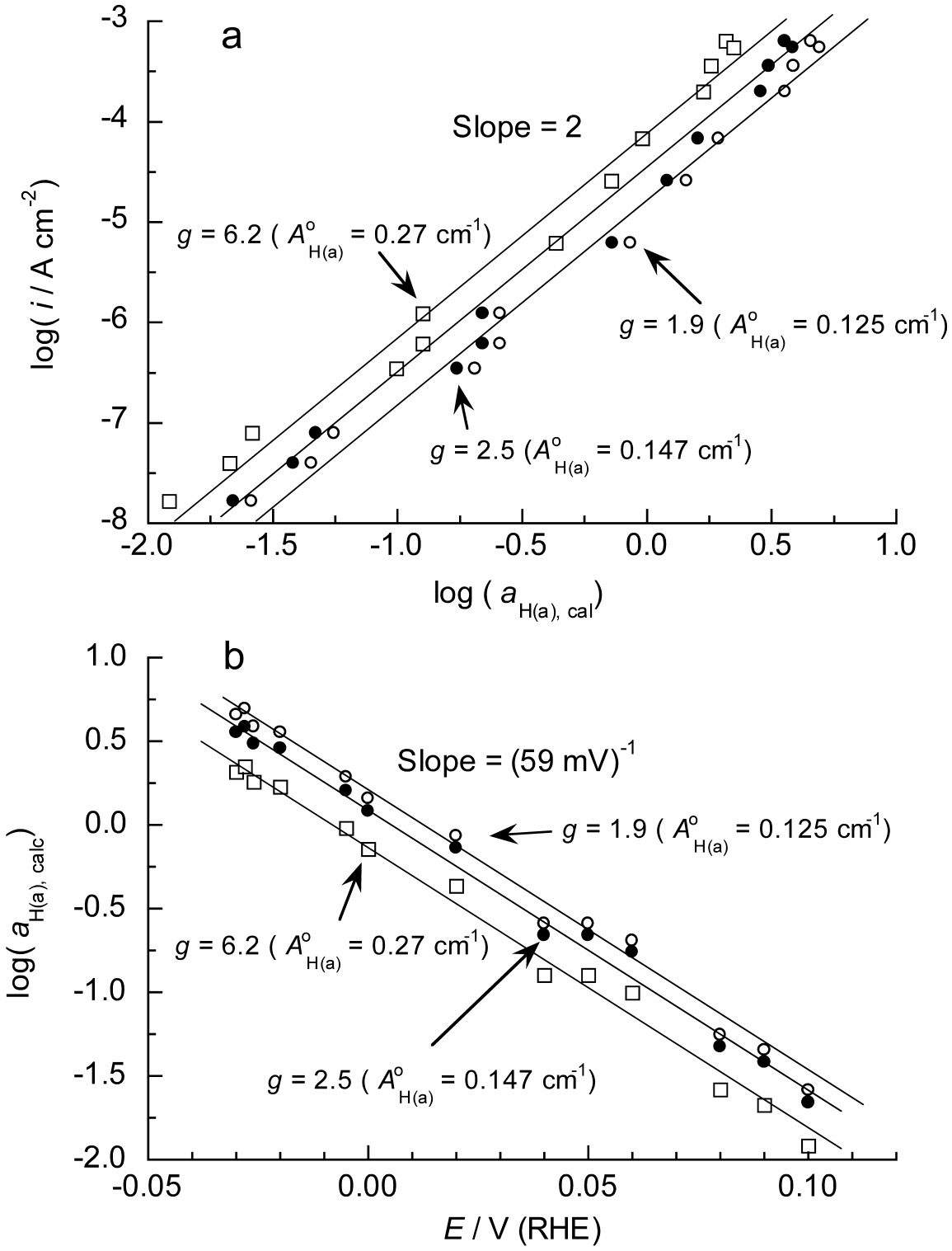

Fig. 13. (a) Log-log plots of the observed current density i and the calculated activities of terminal H $a_{H(a),calc}$, and (b) logarithmic plots of the activities against the applied potential E for the three assumed saturated band intensities ($A^{\circ}_{H(a)}$ = 0.27, 0.147, and 0.125 cm^{-1}). $a_{H(a),calc}$ was calculated from the band intensity data for 0.5 M H_2SO_4 with Eq. 10 by adjusting g value so that the slope of the log i versus log $a_{H(a),\,cal}$ plot becomes 2 for each $A^{\circ}_{H(a)}$ value.

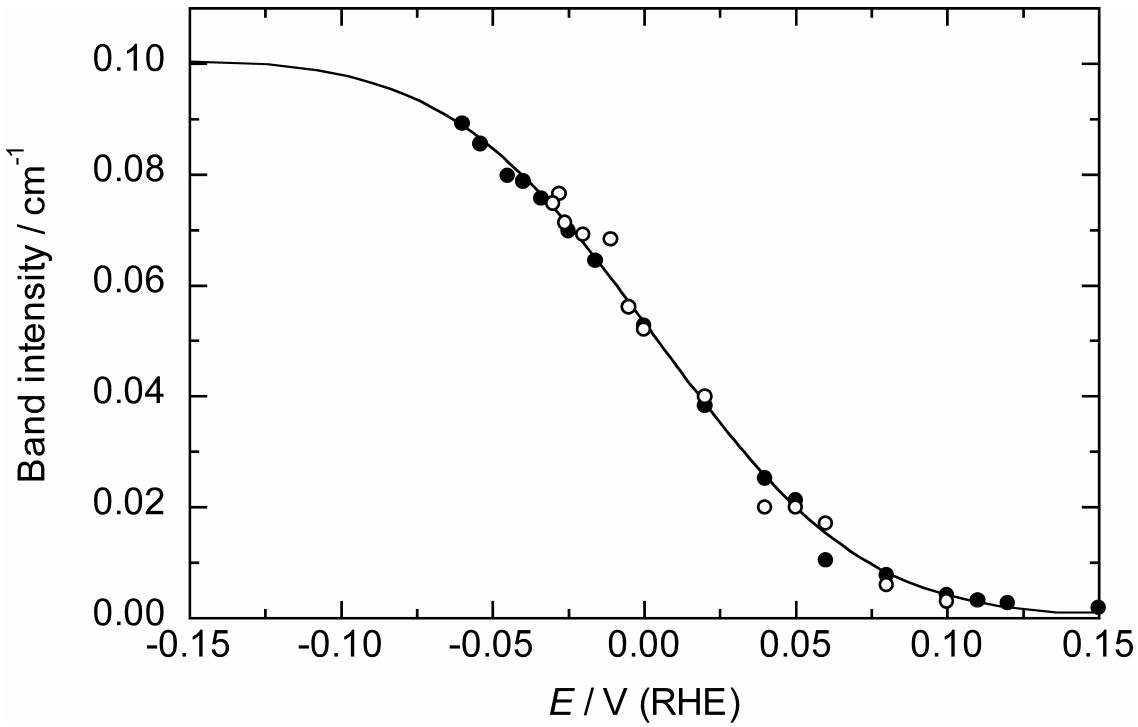

Fig. 14. Least-square fit of the integrated band intensity of terminal H observed in 0.5 (●) and 3 M (○) H_2SO_4 to the electrochemical Frumkin isotherm, Eq. 11. The best fit parameters were g = 1.35 and $A^{\circ}_{H(a)}$ = 0.10 cm^{-1}.